Topologically protected excitons in porphyrin thin films

Citation: Yuen-Zhou, Joel, Semion K. Saikin, Norman Y. Yao, and Alán Aspuru-Guzik. "Topologically Protected Excitons in Porphyrin Thin Films." Nature Materials 13, no. 11 (September 21, 2014): 1026–1032. © 2014 Macmillan Publishers Ltd

As Published: http://dx.doi.org/10.1038/nmat4073

Publisher: Nature Publishing Group

Persistent URL: http://hdl.handle.net/1721.1/95950

Version: Final published version: final published article, as it appeared in a journal, conference proceedings, or other formally published context

ARTICLES
PUBLISHED ONLINE: 21 SEPTEMBER 2014 | DOI: 10.1038/NMAT4073
nature materials

Topologically protected excitons in porphyrin thin films

Joel Yuen-Zhou[1]*, Semion K. Saikin[1,2], Norman Y. Yao[3] and Alán Aspuru-Guzik[1,2]

The control of exciton transport in organic materials is of fundamental importance for the development of efficient light-harvesting systems. This transport is easily deteriorated by traps in the disordered energy landscape. Here, we propose and analyse a system that supports topological Frenkel exciton edge states. Backscattering of these chiral Frenkel excitons is prohibited by symmetry, ensuring that the transport properties of such a system are robust against disorder. To implement our idea, we propose a two-dimensional periodic array of tilted porphyrins interacting with a homogeneous magnetic field. This field serves to break time-reversal symmetry and results in lattice fluxes that mimic the Aharonov–Bohm phase acquired by electrons. Our proposal is the first blueprint for realizing topological phases of matter in molecular aggregates and suggests a paradigm for engineering novel excitonic materials.

On interaction with light, molecules are promoted to excited states, typically referred to as molecular excitons[1] (hereafter referred to as excitons interchangeably). The efficient transport of energy across a molecular array via such excitons is one of the main goals in the design of solar cell devices[2]. This owes to the fact that excitons mediate energy transfer between incoming photons and the electrical current generated on excited-state dissociation[3,4]. In this context, tremendous efforts have been focused on organic photovoltaic materials, which have advantages in terms of production cost, chemical versatility and enhanced absorption properties. However, an important drawback in such organic materials is the presence of a large amount of disorder[5]. Indeed, static disorder arises from structural imperfections in the molecular aggregate which yield local perturbations to the on-site energies as well as to the couplings between molecules. Typically, such disorder induces Anderson localization of the single-particle exciton eigenstates[6], which significantly reduces transport of energy. Although such localizing effects can be partially compensated by the addition of vibrations which help untrap the exciton[7–9], a generic solution remains a challenge.

Our approach to this challenge draws on ideas from the field of disordered electronic systems—in particular, from the phenomenology broadly termed as 'quantum Hall effects' (QHEs; ref. 10). A hallmark of such quantum Hall systems is that they exhibit delocalized current-carrying chiral edge modes. Specifically, the breaking of time-reversal symmetry (TRS) in these systems ensures that there are no counter-propagating modes to backscatter into[11]. Elegant extensions of these ideas include photonic set-ups[12–15] and topological insulators (TI)—materials that preserve TRS but whose edge modes are related to strong spin–orbit coupling[16,17]. We note that organometallic TIs have recently been suggested by Liu and co-workers[18–21], paving the way towards a wider and possibly cheaper group of materials that may exhibit these exotic phenomena.

As QHEs have been posed in the context of electrons and photons, it is natural to inquire whether their excitonic analogue exists. The present Article answers this question positively, by explicitly constructing a minimal model of a Frenkel exciton porphyrin lattice which supports topologically protected edge states when it interacts with a magnetic field. As this effort is already challenging by itself, we limit ourselves to cryogenic temperatures and, therefore, disregard effects of vibrational dephasing of excitons, which we shall study elsewhere. As far as we are aware, this is curiously the first work that addresses the joint effects of both magnetic fields and coherence in molecular exciton transport. Furthermore, this Article is also the first example of topological phases in molecular excitons and, therefore, offers a novel approach to the design of a new generation of materials for more efficient energy harvesting and transport.

The model

Our set-up consists of a two-dimensional periodic array of unsubstituted metalloporphyrins (hereafter referred to just as porphyrins), molecules with D_{4h} symmetry that maintain their planarity owing to their metal centres[22], and which are well-known compounds in photovoltaic applications[23]. These porphyrins are arranged in a square lattice in the xy plane with a unit cell of area $s \times s$ (Fig. 1a), where $s \sim 1/2$–2 nm. The lattice consists of two sublattices, a and b, where the porphyrins are tilted out of the xy plane in ways that depend on two angles per sublattice, θ_i and φ_i $(i = a, b)$, respectively. This two-dimensional lattice can in principle be realized by self-assembly techniques exploiting an already crystalline substrate[24–29], which in our case shall be chosen to avoid exciton quenching processes (an insulating material fulfils this condition[30,31]).

Using a Cartesian vector notation in the 'lab' or array frame throughout the Article, the a sites are located at positions $\mathbf{n}s \equiv (n_x, n_y, 0)s$ for n_x, n_y integers, whereas the b sites are at $(n_x + 1/2, n_y + 1/2, 0)s$. We shall be concerned with the three lowest electronic states in each molecule—namely, its ground state $|g^{(i)}\rangle$ and its degenerate Q-band absorbing in the visible spectrum ($\omega_Q \sim 17{,}350\,\mathrm{cm}^{-1}$; ref. 32), consisting of the orthogonal states $|Q_X^{(i)}\rangle$ and $|Q_Y^{(i)}\rangle$ (we use capital labels for Cartesian coordinates for the molecular frame of each sublattice).

Owing to the degeneracy of the Q-band, the states $|Q_X^{(i)}\rangle$ and $|Q_Y^{(i)}\rangle$ can be arbitrarily defined as long as their transition dipole

[1]Center for Excitonics, Research Laboratory of Electronics, Massachusetts Institute of Technology, Cambridge, Massachusetts 02139, USA, [2]Department of Chemistry and Chemical Biology, Harvard University, Cambridge, Massachusetts 02138, USA, [3]Department of Physics, Harvard University, Cambridge, Massachusetts 02138, USA. *e-mail: joelyuen@mit.edu

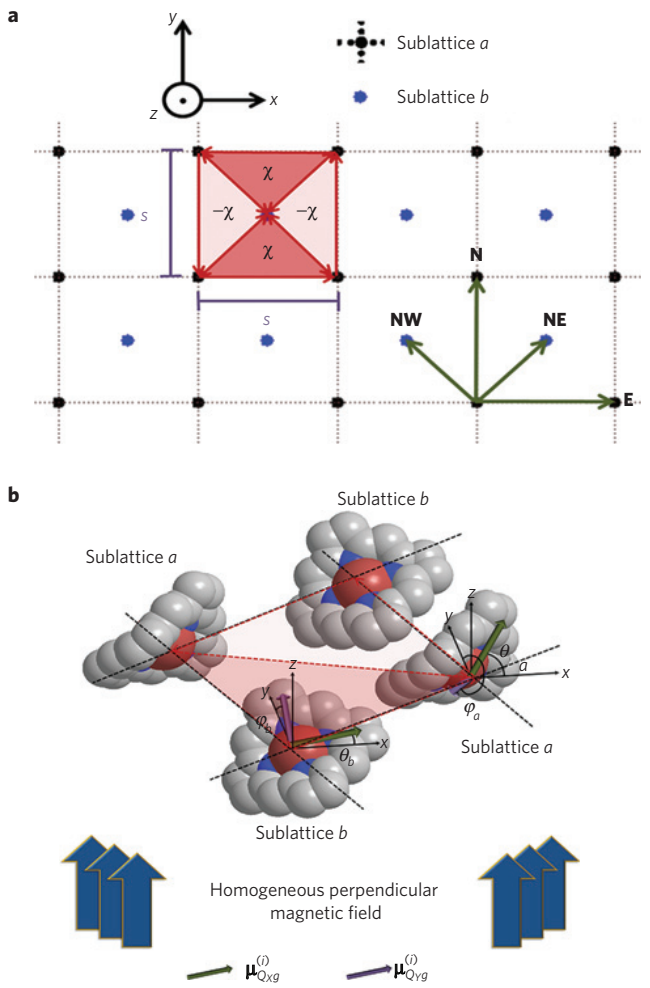

Figure 1 | Porphyrin lattice under a uniform magnetic field. a, The square lattice consists of porphyrins arranged into two sublattices *a* (black) and *b* (blue). A possible unit cell is a square of dimensions $s \times s$. We highlight the fluxes (Berry phases) $\pm\chi$ that the exciton obtains on anticlockwise circulation about each of the minimal three-porphyrin loops. This pattern of fluxes is reminiscent of Haldane's model, where electrons are placed in a lattice under an inhomogeneous magnetic field with no effective magnetic field per unit cell and, yet, manifest non-trivial topological properties. Dipolar coupling between a pair of porphyrins occurs along the **N** (north), **E** (east), **NE** (northeast) and **NW** (northwest) directions, as well as their opposite counterparts. **b**, Magnification of the upper corner of the unit cell in **a**. The actual set-up uses a homogeneous magnetic field. Sublattice *a* differs from sublattice *b* in the orientation angles θ_i, φ_i $(i = a, b)$ of the porphyrins with respect to the *x* and *y* axes. Each porphyrin consists of two transition dipoles $\boldsymbol{\mu}^{(i)}_{Qxg}$ and $\boldsymbol{\mu}^{(i)}_{Qyg}$ in the plane of the molecules. The anisotropic character of dipolar interactions together with the magnetic field makes the exciton hoppings along the northeast and the northwest directions different enough to obtain a non-zero flux χ.

moments with respect to $|g^{(i)}\rangle$ constitute an orthogonal set of vectors of equal magnitude d spanning the plane of each porphyrin. We denote the transition dipole operator for a porphyrin in sublattice i by $\boldsymbol{\mu}^{(i)} = \boldsymbol{\mu}^{(i)}_{Qxg}|Q^{(i)}_X\rangle\langle g^{(i)}| + \boldsymbol{\mu}^{(i)}_{Qyg}|Q^{(i)}_Y\rangle\langle g^{(i)}| + \text{c.c.}$, where $\boldsymbol{\mu}^{(i)}_{Qxg} = \boldsymbol{\mu}^{(i)}_{gQx}$ and $\boldsymbol{\mu}^{(i)}_{Qyg} = \boldsymbol{\mu}^{(i)}_{gQy}$ are chosen such that $\boldsymbol{\mu}^{(i)}_{Qxg}$ has zero projection along the y axis, and $\boldsymbol{\mu}^{(i)}_{Qyg}$ is orthogonal to it:

$$\boldsymbol{\mu}^{(i)}_{Qxg} = d(\cos\theta_i, 0, \sin\theta_i)$$

$$\boldsymbol{\mu}^{(i)}_{Qyg} = d(-\sin\varphi_i \sin\theta_i, \cos\varphi_i, \sin\varphi_i \cos\theta_i)$$

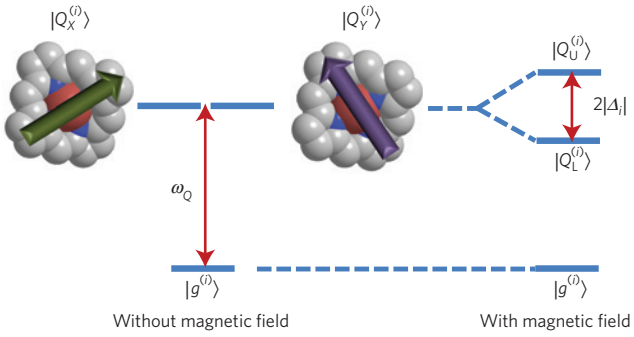

Figure 2 | Porphyrin under a magnetic field. In the absence of a magnetic field, a porphyrin can be thought of as three-level molecule with a ground state $|g^{(i)}\rangle$ and a *Q*-band formed by two degenerate excited states $|Q^{(i)}_X\rangle$ and $|Q^{(i)}_Y\rangle$ at an energy ω_Q. A magnetic field **B** breaks time-reversal symmetry, as well as the degeneracy via a Zeeman splitting $2|\Delta_i|$, yielding lower $|Q^{(i)}_L\rangle$ and upper $|Q^{(i)}_U\rangle$ eigenstates with definite angular momentum along $\mathbf{Z}_i$. Here, *i* denotes different sublattices $i = a, b$.

where $d \sim 2$–8 D depending on the chemical environment of the porphyrins[33]. These vectors define molecular frames for each sublattice, with Cartesian unit vectors $\mathbf{X}_i = \boldsymbol{\mu}^{(i)}_{Qxg}/d$, $\mathbf{Y}_i = \boldsymbol{\mu}^{(i)}_{Qyg}/d$, and $\mathbf{Z}_i = \mathbf{X}_i \times \mathbf{Y}_i$. Also, in general $(\theta_a, \varphi_a) \neq (\theta_b, \varphi_b)$, so the tilting angles distinguish the sublattices.

Before dealing with the dipolar interactions between the different porphyrins, we consider their Zeeman interaction with a perpendicular and homogeneous magnetic field $\mathbf{B} = (0, 0, B)$ (see ref. 34; Fig. 2):

$$H^{(i)} = H^{(i)}_0 - \mu_0 \mathbf{B} \cdot (\mathbf{L}^{(i)} + 2\mathbf{S}^{(i)}) \qquad (1)$$

Here, $H^{(i)}_0 = \omega_Q(|Q^{(i)}_X\rangle\langle Q^{(i)}_X| + |Q^{(i)}_Y\rangle\langle Q^{(i)}_Y|)$ is the bare Hamiltonian of each porphyrin, $\mu_0 = 0.47\ \text{cm}^{-1}\,\text{T}^{-1}$ is the Bohr magneton, and $\mathbf{L}^{(i)}$ and $\mathbf{S}^{(i)}$ are the electronic orbital angular momentum and spin of the *i*th porphyrin. Each of the three states per molecule is a singlet state with $\mathbf{S}^{(i)} = 0$. It is valid to regard the porphyrins as approximate rings in the X_iY_i planes occupied by 18 electrons[32,34,35]. This implies that the solutions to equation (1) are states with approximately good angular momentum quantum number $L^{(i)}_Z = \pm m$ perpendicular to the plane of the molecules at $\mathbf{Z}_i$ for integer m (here $\hbar = 1$). In particular, we have $L^{(i)}_Z|g^{(i)}\rangle = 0$ and $L^{(i)}_Z|Q^{(i)}_\pm\rangle \equiv L^{(i)}_Z(|Q^{(i)}_X\rangle \pm i|Q^{(i)}_Y\rangle)/\sqrt{2} = \pm 9|Q_\pm\rangle$, yielding $H^{(i)}|g^{(i)}\rangle = 0$ and $H^{(i)}|Q^{(i)}_\pm\rangle = (\omega_Q \mp \Delta_i)|Q^{(i)}_\pm\rangle$, where half of the Zeeman splitting is given by $\Delta_i \equiv 9\mu_0 B_z \kappa_i$, and we have used $\kappa_i \equiv \mathbf{z} \cdot \mathbf{Z}_i = \cos\theta_i \cos\varphi_i$. That is, under a magnetic field, the degenerate *Q*-band in each porphyrin splits into two Zeeman levels $|Q^{(i)}_\pm\rangle$ with different energies. Notice that as a result of TRS breaking, their coefficients in terms of the 'bare' states $|Q^{(i)}_X\rangle$ and $|Q^{(i)}_Y\rangle$ are in general complex. Although not essential, we simplify the model by fixing the projection of the magnetic field on both sublattices to be a constant $|\kappa_i| = \kappa \neq 0$, yielding a constant Zeeman splitting throughout $|\Delta_i| = \Delta$. There is, however, a possibly different ordering of the $|Q^{(i)}_\pm\rangle$ states, depending on the sign of $B_z\kappa_i$. With this in mind, each porphyrin has states of energy $\omega_L \equiv \omega_Q - \Delta$ and $\omega_U \equiv \omega_Q + \Delta$, which we call the lower and upper energy states $|Q^{(i)}_L\rangle$ and $|Q^{(i)}_U\rangle$, and $(L, U) = (+, -)$ if $B_z\kappa_i > 0$ and $(L, U) = (-, +)$ otherwise. Working under a magnetic field of $|B_z| = 10$ T, this splitting attains a value of $2\Delta \sim 84\ \text{cm}^{-1}$, which is confirmed by magnetic dichroism experiments[32] (the reference reports half of the actual splitting due to isotropic averaging). It is clear from this model that other chromophores with similar electronic structure, such as metallophthalocyanines[36], can be used instead of metalloporphyrins.

We now turn our attention to interactions between Zeeman levels across the lattice, which we characterize with the energy scale J,

such that $J \ll 2\Delta$. We are interested only in 'single-excitation' effects, which can be described by the following Hamiltonian:

$$\begin{aligned}\mathscr{H}_{\mathrm{L}} = \sum_{n} \big(&\omega_{\mathrm{L}}(a^{\dagger}_{\mathbf{n}}a_{\mathbf{n}} + b^{\dagger}_{\mathbf{n}}b_{\mathbf{n}}) \\ &+ J_{ab,\mathbf{NE}}(a^{\dagger}_{\mathbf{n}+\mathbf{NE}}b_{\mathbf{n}} + a^{\dagger}_{\mathbf{n}-\mathbf{NE}}b_{\mathbf{n}}) \\ &+ J_{ab,\mathbf{NW}}(a^{\dagger}_{\mathbf{n}+\mathbf{NW}}b_{\mathbf{n}} + a^{\dagger}_{\mathbf{n}-\mathbf{NW}}b_{\mathbf{n}}) \\ &+ J_{aa,\mathbf{E}}a^{\dagger}_{\mathbf{n}+\mathbf{E}}a_{\mathbf{n}} + J_{aa,\mathbf{N}}a^{\dagger}_{\mathbf{n}+\mathbf{N}}a_{\mathbf{n}} \\ &+ J_{bb,\mathbf{E}}b^{\dagger}_{\mathbf{n}+\mathbf{E}}b_{\mathbf{n}} + J_{bb,\mathbf{N}}b^{\dagger}_{\mathbf{n}+\mathbf{N}}b_{\mathbf{n}}\big) + \text{c.c.} \qquad (2)\end{aligned}$$

Here, $a^{\dagger}_{\mathbf{n}}$ and $b^{\dagger}_{\mathbf{n}}$ are creation operators for excitations $|Q^{(i)}_{\mathrm{L}}\rangle$ located at $\mathbf{n}s$ for $i=a$ and at $(n_x+1/2, n_y+1/2, 0)s$ for $i=b$. We have considered only nearest-neighbour (NN, $J_{ab,\mathbf{NE}}$, $J_{ab,\mathbf{NW}}$) and next-nearest-neighbour (NNN, $J_{aa,\mathbf{E}}$, $J_{bb,\mathbf{E}}$, $J_{aa,\mathbf{N}}$, $J_{bb,\mathbf{N}}$) dipolar couplings, labelled by the vector $\mathbf{V}$ connecting the two interacting dipoles, $\mathbf{N}=(0,1,0)$ (north), $\mathbf{E}=(1,0,0)$ (east), $\mathbf{NE}=1/2(1,1,0)$ (northeast) and $\mathbf{NW}=1/2(-1,1,0)$ (northwest). The analogous Hamiltonian $\mathscr{H}_{\mathrm{U}}$ can be similarly constructed using the states $|Q^{(i)}_{\mathrm{U}}\rangle$. It can be checked that NNN couplings $J_{ii,\mathbf{V}}$ are real-valued, whereas NN couplings $J_{ab,\mathbf{V}}$ are complex-valued in general owing to TRS breaking through the Zeeman effect (Methods). Importantly, the complex phases in these couplings do not represent physical observables on their own, as they can be modified via gauge transformations. Yet, the Berry phases accumulated in closed loops, and in particular those obtained by encircling the minimal three-porphyrin-loops are gauge invariant modulo 2π and, therefore, have observable consequences. Figure 1 shows that, in each unit cell, two of the anticlockwise loops yield a phase $\chi \equiv \arg(J^{*}_{ab,\mathbf{NW}}J_{aa,\mathbf{NE}}J_{ab,\mathbf{E}}) = -\arg(J_{ab,\mathbf{NW}}J_{ab,\mathbf{E}})$ and the other two yield the opposite phase $\arg(J_{ab,\mathbf{SE}}J_{ba,\mathbf{SW}}J_{aa,\mathbf{N}}) = -\chi$. A peculiar feature of dipolar interactions between the tilted porphyrins is its anisotropic character, which renders $\arg(J_{ab,\mathbf{NE}})$ different from $\arg(J_{ab,\mathbf{NW}})$, except for a measure-zero set of critical orientations, and therefore keeps χ finite for every set of tilting angles as long as the magnetic field is on. This observation is also at the core of recent work on topological phases in dipolar spins for optical lattices[37,38]. Thus, equation (2) has the same structure as the Hamiltonian for electrons in a lattice under a perpendicular and inhomogeneous magnetic field threading net fluxes $\pm\chi$ across the minimal loops, but a net zero magnetic flux per unit cell and, therefore, across the lattice. Let us summarize what we have done so far: we have constructed a model where Frenkel excitons (quasiparticles with no net charge) under a homogeneous magnetic field behave as if they were electrons (particles with charge) in an inhomogeneous magnetic field. Hence, this model is a square lattice version of Haldane's honeycomb problem and, therefore, expected to exhibit non-trivial topological properties, in particular, chiral Frenkel exciton edge states which are robust against disorder[39]. This realization is the main finding of the Article.

Topological characterization of exciton phases

On fixing the Zeeman splitting $2\Delta = |B_z|\kappa$, the unit cell distance s and transition dipole moment strength d, there is a two-dimensional parameter space which is left to be explored by varying the tilting angles θ_a and θ_b (the possible values of φ_a and φ_b are fixed by κ). These parameters suffice to provide a topological characterization of $\mathscr{H}_{\nu}$ via the Chern numbers $\mathscr{C}_{\nu}$ for $\nu = \mathrm{L},\mathrm{U}$ (see Methods for details)[40]. The physical meaning of $\mathscr{C}_{\nu}$ is the following: its sign denotes the chirality of the edge states (in our convention, positive for clockwise and negative for anticlockwise); its magnitude is equal to the (integer) number of edge states per value of quasimomentum (given open boundary conditions (OBC) along one axis).

A computational exploration of the parameter space reveals that $\mathscr{C}_{\nu} = \pm 1$ for every tilting configuration that respects the specified constraints, except for a measure-zero set of parameters which yields $\mathscr{C}_{\nu} = 0$, when the two sublattices become identical at the critical values $\theta_b = \pm\theta_a, \pi \pm \theta_a$, and the gap between the two bands in each $\mathscr{H}_{\nu}$ closes. Furthermore, we can see that $\langle \mathbf{n}^{(i)}_{\mathrm{L}}|J|\mathbf{m}^{(j)}_{\mathrm{L}}\rangle = \langle \mathbf{n}^{(i)}_{\mathrm{U}}|J|\mathbf{m}^{(j)}_{\mathrm{U}}\rangle^{*}$, so that every minimal loop that features a flux χ in $\mathscr{H}_{\mathrm{L}}$ (see previous section) features the opposite flux $-\chi$ in $\mathscr{H}_{\mathrm{U}}$, implying that $\mathscr{C}_{\mathrm{L}} = -\mathscr{C}_{\mathrm{U}}$. Therefore, both clockwise and anticlockwise edge currents show up in every topologically non-trivial configuration, except that they come at different energies separated by $\sim 2\Delta$. Yet, it is possible to control the energy level ordering of these chiral currents by tuning the direction of the magnetic field, as our numerical studies show that $\mathscr{C}_{\mathrm{L}} = -\mathrm{sgn}(B_z)$. This picture contrasts radically with that of the integer QHE in a two-dimensional electron gas in the absence of a lattice, where the direction of the magnetic field imposes a fixed direction of cyclotron motion of the electrons and, therefore, also the chirality of all the edge currents. As an illustration of these ideas, Fig. 3 shows the topological phase diagram for the $\kappa = 1/2$, $B_z > 0$ case. Given κ and the fact that $\cos\theta_i, \cos\varphi_i \in [-1,1]$, we must restrict $\theta_i \in [-a\cos\kappa, a\cos\kappa] \cup [\pi - a\cos\kappa, \pi + a\cos\kappa]$. The remainder of the angles violate the condition of fixed $|\kappa_i| = \kappa$, but a fraction of them still contains topologically non-trivial phases. The characterization of this precise fraction is beyond the scope of this Article, but will be explored in the extension of this work.

Let us be more explicit by considering a particular point $(\theta_a, \varphi_a) = (-\pi/3, 0)$ and $(\theta_b, \varphi_b) = (0, \pi/3)$ of this phase diagram, where $-\kappa_a = \kappa_b = \kappa = 1/2$. We refer the reader to Fig. 4, which is organized in panels a and b, each of them containing three parts. We show results for $\mathscr{H}_{\mathrm{L}}$, with the conclusions for $\mathscr{H}_{\mathrm{U}}$ being analogous except for opposite chirality of edge currents (energies and dipoles are plotted in units of J and d). In Fig. 4a, we show the ideal case where the tilting angles of the porphyrins are placed exactly at the mentioned values. In Fig. 4b, we show a specific realization of disorder where each of the site angles has been randomized with Gaussian noise with 0.13π standard deviation about the ideal values. The left panels show the current density for a particular eigenstate of $\mathscr{H}_{\mathrm{L}}$ under OBC. These currents are concentrated along the edges of the material, so they correspond to exciton edge states and they flow clockwise, consistent with $\mathscr{C}_{\mathrm{L}} = -1$. Interestingly, in the disordered lattice, regardless of the tilting randomization, the edge current and its chirality are still preserved. To accentuate this effect, we add a potential barrier at the left corner of the lattice, simulating an obstacle. The exciton current simply circumvents the obstacle, keeping its delocalization throughout, exemplifying the properties of topological protection. We have shown lattices with approximately 200 porphyrins, corresponding to a reasonable number of molecules that remain coherently coupled at cryogenic temperatures[41]; this number might even be a lower bound, as coherence size is limited by coupling to vibrations and disorder, but the latter is somehow circumvented in these topological systems. The centre panels offer the energy diagrams of the respective lattices under OBC along y and periodic boundary conditions (PBC) along x. For the ideal lattice, this corresponds to two bulk bands as a function of quasimomentum k_x together with edge states that span the gap between the latter from $E \approx -2J$ to $2J$. The dispersion of the edge states is positive and negative, corresponding to currents at the bottom and top edges of the lattice. Note that these states of opposite dispersion merge at $k_x = 0$ with the bulk bands. The analogous band diagram is unavailable for the disordered lattice owing to lack of translational symmetry, so we simply collapse all the eigenenergies in the same line. A study of the eigenstates reveals that the eigenstates between $E \approx -0.8J$ and $0.4J$ exhibit mostly edge character. We comment

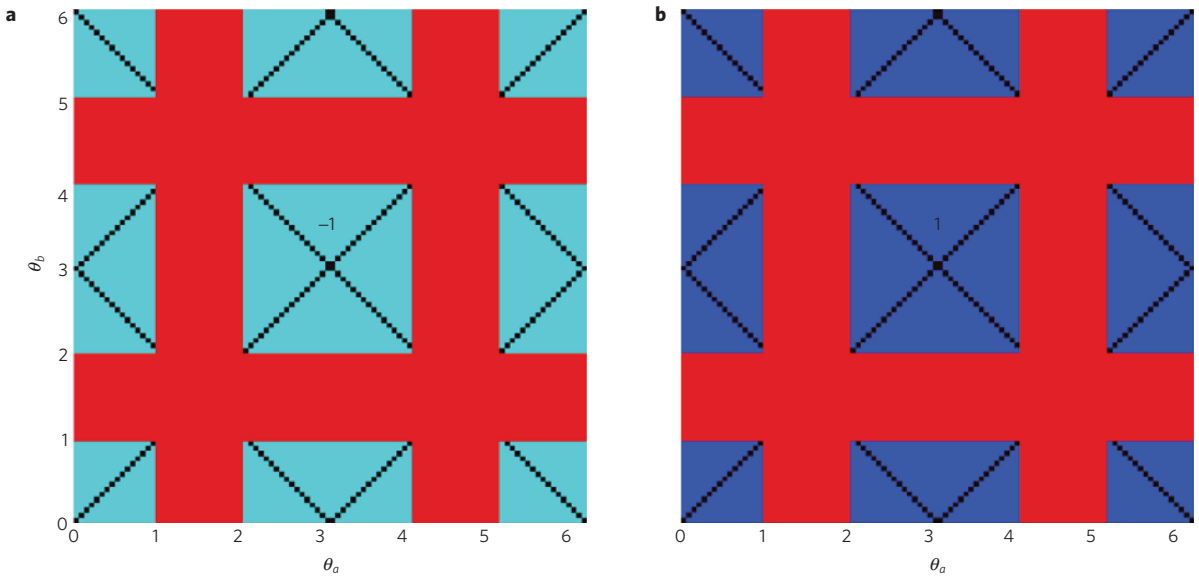

Figure 3 | Phase diagram of exciton topological phases. We fix $\kappa = |\cos\theta_i \cos\varphi_i| = 1/2$, the projection of the magnetic field $B_z > 0$ with the porphyrin rings and we study the resulting topological phases as a function of the tilting angles θ_i ($\pm\varphi_i$ is fixed by κ, $i = a, b$). Red regions are parameters for which values of θ_i and φ_i cannot yield $\kappa = 1/2$, and, therefore, are not considered. **a**,**b**, Diagrams for the upper and lower energy exciton Hamiltonians $\mathscr{H}_X$ ($v = \mathrm{L}, \mathrm{U}$), respectively. Light and dark blue regions denote topologically non-trivial phases with Chern number $\mathscr{C}_v$ equal to -1 and 1, exhibiting edge states with anticlockwise and clockwise exciton currents, respectively. Switching the direction of the magnetic field to $B_z < 0$ inverts these chiralities. Black lines correspond to topologically trivial phases with $\mathscr{C}_v = 0$ and are located along the critical parameters $\theta_b = \pm\theta_a, \pi \pm \theta_a$, where the two sublattices become identical and the gaps of the respective Hamiltonians vanish.

that, in fact, edge states seem to survive up to a large amount of disorder—namely, with noise distributed at $\pi/6$ standard deviation. Finally, the right panels show the linear absorption spectra of the lattice with OBCs along both directions x and y. In analogy with J- and H-aggregates, most of their oscillator strength is concentrated in relatively few bulk eigenstates in the ideal lattice, although neither at top or bottom of the bands, as opposed to the simple quasi-one-dimensional scenario[41]. This renders the edge states in the top panel mostly dark, with the brightest edge state absorbing only 2.7% of the highest absorption peak in the spectrum. This fact is consistent with the observation that, in the dipole approximation, only states with $k_x = 0$ are bright, but there are no such states located at the edge in our particular model. Counterintuitively, moderate amounts of disorder provide a solution to this problem, as the edge states in this lattice borrow enough oscillator strength from the original bulk states to yield peaks in the absorption spectrum that are more experimentally accessible[6], with some edge absorption peaks attaining intensities of about 26% of that of the highest bulk bands. Hence, linear absorption spectra provide a coarse signature of the edge states, although no actual confirmation of their topological character. To experimentally probe the latter, we forsee the use of near-field optical microscopy, where a metal tip locally creates excitons at the edge of the lattice and spatially resolved fluorescence is used to detect the chirality of the resulting exciton currents[42]. This phenomenology could also be inferred using far-field microscopy, albeit at a coarser spatial resolution[43]. The detailed proposal for the experimental preparation and detection of the edge exciton currents is a delicate subject on its own, and will be reported in an extension of this work. Similarly, as noted at the beginning of the Article, we have omitted the discussion of interactions between excitons and molecular vibrations, regarding them as weak compared to the coupling J. Assuming a thermal scale $k_B T$ for the former, where k_B is Boltzmann's constant and T is the temperature, we require the hierarchy of energy scales $k_B T \ll J \ll 2\Delta$, which amounts to cryogenic values of $T \approx 4$ K, given the values of J and 2Δ in this Article. We emphasize that the restriction to cryogenic temperatures is not a fundamental one. It arises from the modest values of Zeeman splitting 2Δ attained at realistic magnetic fields, and not from J, which can assume large values on appropriate chemical functionalization[44]. Hence, if 2Δ can be enhanced otherwise (for instance, via optical dressing), the domain validity of the model can be pushed to much higher temperatures. For arbitrary exciton–vibrational couplings, the current model needs to be adapted and, at present, it is not clear under which general conditions topologically non-trivial phases will survive, as vibrations might suppress them if they serve as a thermal dephasing bath, but may also sustain them non-trivially if they act as a non-Markovian bath.

Summary and conclusions

This Article introduces the concepts of topological phases to the field of molecular excitonics. It does so by explicitly constructing a topologically non-trivial model for Frenkel excitons in a two-dimensional lattice of porphyrins. Important ingredients of the model are the presence of two orbitally polarized excitons per porphyrin, the interaction of the lattice with a perpendicular magnetic field, the anisotropy of dipolar interactions between excitons, and the two-sublattice configuration of tilted porphyrins, yielding two pairs of exciton energy bands. The proposed system is a variant of the Haldane model, yielding one-way exciton edge states that are robust against disorder, as we have shown by calculations of topological invariants of the resulting energy bands as well as by explicit simulations of finite lattices. An experimental signature of these edge states is given by linear absorption spectra, although the experimental confirmation of their topological character requires more careful experiments, which will be proposed elsewhere.

We believe that our work is just one of many examples yet to be studied of a new pool of strategies to engineer robust 'exciton wires' that can efficiently transport light-harvested energy. Among some specific future directions, we plan to explore whether the

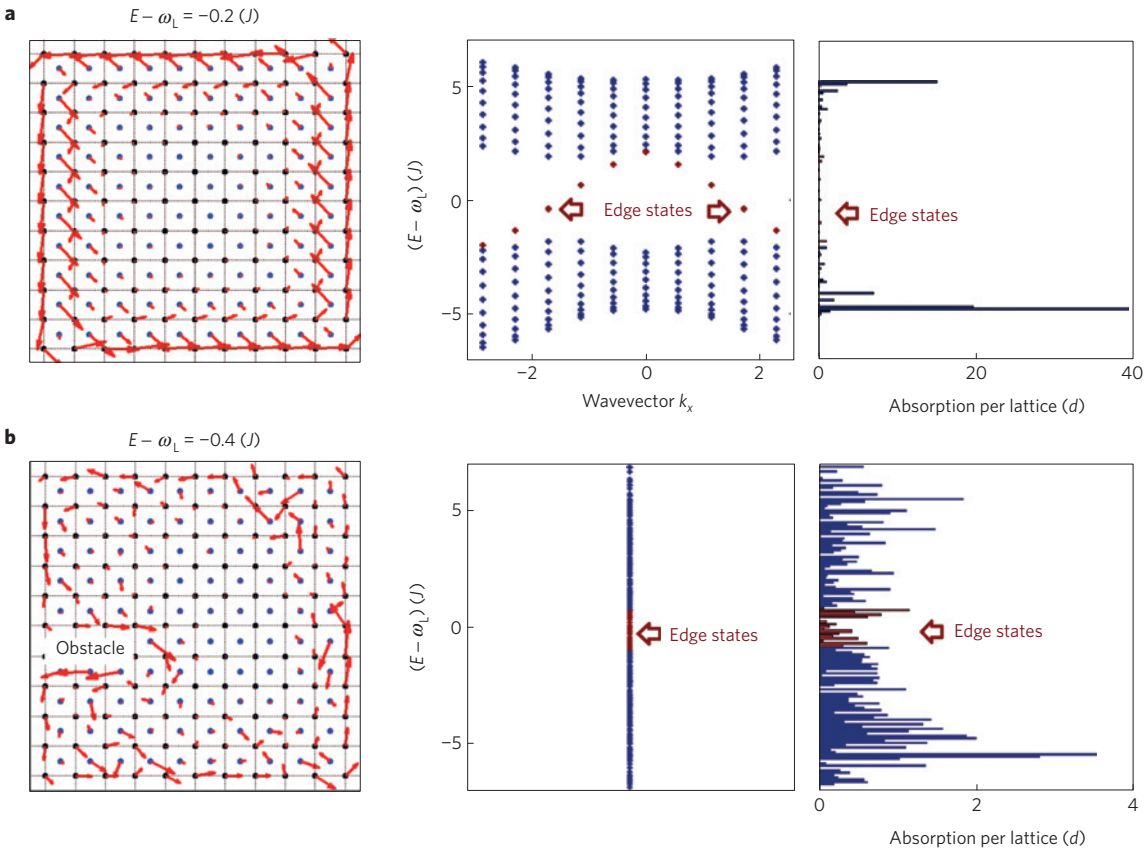

Figure 4 | Eigenstates of the lower energy Hamiltonian $\mathscr{H}_L$ for porphyrin tilting angles $(\theta_a,\varphi_a)=(-\pi/3,0)$ and $(\theta_b,\varphi_b)=(0,\pi/3)$ and magnetic field $B_z>0$. These parameters yield a $\mathscr{C}_L=-1$ phase, which exhibits anticlockwise edge exciton currents. **a**, Ideal lattice without disorder. The left panel shows the current density (red arrows) for a particular edge state. The centre panel depicts the band diagram with bulk (blue) and edge (red) states. Positive and negative dispersion for the edge states correspond to right and left moving states that are localized at the lower and upper edges of the sample. The right panel shows the absorption spectrum of the lattice, indicating that most of the oscillator strength is primarily concentrated in a few bulk states. **b**, The analogous panels for a disordered lattice, where the tilting angles for each porphyrin site are randomized with noise distributed at a 0.13π standard deviation. Furthermore, an obstacle (potential barrier) is added on the left-hand corner of the lattice. Note that the edge current density persists with disorder and, in fact, circumvents the obstacle, remaining delocalized across the edge. In the centre panel, we show the corresponding density of states, highlighting the region of energy where the states still have a substantial edge character. The right panel shows the absorption spectrum, where the disorder redistributes the oscillator strength of the ideal lattice. The edge states borrow enough oscillator strength to be measured experimentally in a linear absorption experiment.

coupling of excitons with various spatially shaped electromagnetic fields, such as plasmons and optical cavities, renders topologically non-trivial motion of excitons. Furthermore, connections between this work and theories of TRS breaking in quantum transport remain to be explored[45,46]. Another intriguing extension of this work is the TRS version of the model, where no magnetic field is present. Regarding the Q-band of each porphyrin as a pseudospin, the anisotropy of the dipolar couplings may be regarded as a pseudospin–orbit coupling, yielding excitonic TI analogues or, more precisely, analogues of topological crystalline insulators, which are a new class of materials where orbital degrees of freedom together with spatial symmetries of the lattice render topologically non-trivial band structures[47,48]. Topological excitonics is an exciting frontier of soft condensed matter and materials physics research.

Methods

Dipolar interactions between Zeeman levels. Let us elaborate on the derivation of equation (2). We are interested only in weak, single-excitation effects, so it is convenient to introduce the global ground state $|G\rangle\equiv|g\rangle\cdots|g\rangle$ as well as the single-site excited states $|\mathbf{n}_q^{(i)}\rangle\equiv|g\rangle\cdots|Q_q^{(i)}\rangle\cdots|g\rangle$, with $q=X,Y,\mathrm{L},\mathrm{U}$, where every porphyrin in the lattice is in the ground state except for the porphyrin in sublattice i, located at $\mathbf{n}s$ or $(n_x+1/2,n_y+1/2,0)s$ (depending on whether $i=a$ or b, respectively), which is in the $|Q_q^{(i)}\rangle$ excited state. Couplings between the bare porphyrin sites in the lattice are well approximated by the classical real-valued dipole–dipole interaction[33]

$$\langle\mathbf{n}_q^{(i)}|\mathscr{J}|\mathbf{m}_r^{(j)}\rangle\approx\frac{\eta}{|\mathbf{R}_{nm}^{(ij)}|^3}\left(\boldsymbol{\mu}_{Q_qg}^{(i)}\cdot\boldsymbol{\mu}_{Q_rg}^{(j)}-3(\boldsymbol{\mu}_{Q_qg}^{(i)}\cdot\mathbf{e}_{nm}^{(ij)})(\boldsymbol{\mu}_{Q_rg}^{(j)}\cdot\mathbf{e}_{nm}^{(ij)})\right)\qquad(3)$$

Here, $\eta=5.04\,\mathrm{cm}^{-1}(\mathrm{nm}^3\,\mathrm{D}^{-2})$ (we have set the index of refraction to 1), $q,r=X,Y$, and $\mathbf{R}_{nm}^{(ij)}$ is the position vector pointing from the $\mathbf{n}$th porphyrin of sublattice i to the $\mathbf{m}$th porphyrin of sublattice j, and $\mathbf{e}_{nm}^{(ij)}=\mathbf{R}_{nm}^{(ij)}/|\mathbf{R}_{nm}^{(ij)}|$. To establish an energy scale associated with these interactions, we define $J\equiv fd^2/s^3$, which for $d=3\,\mathrm{D}$ and $s=2\,\mathrm{nm}$ gives $J=5.7\,\mathrm{cm}^{-1}$—thus, $J\ll2\Delta$ and the Zeeman spitting is much larger than the dipolar couplings, consistent with our assumptions. Couplings between Zeeman levels follow from equation (3) and the appropriate change of basis

$$\langle\mathbf{n}_u^{(i)}|\mathscr{J}|\mathbf{m}_v^{(j)}\rangle=\sum_{q,r=X,Y}\langle Q_u^{(i)}|Q_q^{(i)}\rangle\langle\mathbf{n}_q^{(i)}|\mathscr{J}|\mathbf{m}_r^{(j)}\rangle\langle Q_r^{(j)}|Q_v^{(j)}\rangle$$

where $u,v=\mathrm{L},\mathrm{U}$. The various coupling terms in equation (2) are given by $J_{ij,\mathbf{V}}\equiv\langle(\mathbf{n}+\mathbf{V})_L^{(i)}|\mathscr{J}|\mathbf{n}_L^{(j)}\rangle=\langle(\mathbf{n}-\mathbf{V})_L^{(i)}|\mathscr{J}|\mathbf{n}_L^{(j)}\rangle$ for the different direction vectors $\mathbf{V}$. From the energetic considerations above, we need to include couplings within each band of $|Q_L^{(i)}\rangle$ or $|Q_U^{(i)}\rangle$ states, but not between them. Therefore, we may write a Frenkel exciton Hamiltonian for the total lattice that reads as $\mathscr{H}=\mathscr{H}_L+\mathscr{H}_U$. In particular, $\mathscr{H}_L$, which is explicitly given by equation (2), is constructed using the lower energy states $|Q_L^{(i)}\rangle$, or alternatively $|\mathbf{n}_L^{(i)}\rangle$, by

introducing the second quantized notation for each sublattice $a_{\mathbf{n}}^{\dagger}|G\rangle = |\mathbf{n}_{\mathrm{L}}^{(a)}\rangle$ and $b_{\mathbf{n}}^{\dagger}|G\rangle = |\mathbf{n}_{\mathrm{L}}^{(b)}\rangle$.

Topological characterization of the lattice Hamiltonian $\mathscr{H}_{\mathrm{L}}$. By imposing periodic boundary conditions (PBC) along x and y, $\mathscr{H}_{\mathrm{L}}$ can be rewritten in quasimomentum $\mathbf{k}$-space using the operators $a_{\mathbf{k}}^{\dagger} = 1/\sqrt{N_x N_y}\sum_{\mathbf{n}} a_{\mathbf{n}}^{\dagger} e^{-i\mathbf{k}\cdot\mathbf{n}}$ and $b_{\mathbf{k}}^{\dagger} = 1/\sqrt{N_x N_y}\sum_{\mathbf{n}} b_{\mathbf{n}}^{\dagger} e^{-i\mathbf{k}\cdot\mathbf{n}}$, where N_x and N_y are the number of unit cells along the x and y directions, and $\mathbf{k} = (k_x, k_y)$ can take values in the Brillouin zone $-\pi \le k_x, k_y < \pi$ in discrete steps of $\Delta k_x = 2\pi/N_x$ and $\Delta k_y = 2\pi/N_y$, respectively. In terms of these operators, equation (2) becomes $\mathscr{H}_{\mathrm{L}} = \sum_{\mathbf{k}} (a_{\mathbf{k}}^{\dagger}\ \ b_{\mathbf{k}}^{\dagger}) H(\mathbf{k}) (a_{\mathbf{k}}\ \ b_{\mathbf{k}})^{\mathrm{T}}$, where $H(\mathbf{k}) = \mathbf{d}(\mathbf{k})\cdot\boldsymbol{\sigma} + f(\mathbf{k})I$ describes a two-band model. Here, $\boldsymbol{\sigma} = (\sigma_x, \sigma_y, \sigma_z)$ and I are the vector of Pauli spin matrices and the two-by-two identity matrix, and $\mathbf{d}(\mathbf{k}) = (d_x(\mathbf{k}), d_y(\mathbf{k}), d_z(\mathbf{k}))$ and $f(\mathbf{k})$ are a $\mathbf{k}$-dependent vector and scalar given by

$$d_x(\mathbf{k}) = A_1 \cos\left(\frac{k_x + k_y}{2}\right) + A_2 \cos\left(\frac{k_x - k_y}{2}\right) \tag{4a}$$

$$d_y(\mathbf{k}) = B_1 \cos\left(\frac{k_x + k_y}{2}\right) + B_2 \cos\left(\frac{k_x - k_y}{2}\right) \tag{4b}$$

$$d_z(\mathbf{k}) = C_1 \cos(k_x) + C_2 \cos(k_y) \tag{4c}$$

$$f(\mathbf{k}) = D_1 \cos(k_x) + D_2 \cos(k_y) \tag{4d}$$

where $A_1 = 2\Re J_{ab,\mathrm{NE}}$, $A_2 = 2\Re J_{ab,\mathrm{NW}}$, $B_1 = -2\Im J_{ab,\mathrm{NE}}$, $B_2 = -2\Im J_{ab,\mathrm{NW}}$, $C_1 = J_{aa,\mathrm{E}} - J_{bb,\mathrm{E}}$, $C_2 = J_{aa,\mathrm{N}} - J_{bb,\mathrm{N}}$, $D_1 = J_{aa,\mathrm{E}} + J_{bb,\mathrm{E}}$, and $D_2 = J_{aa,\mathrm{N}} + J_{bb,\mathrm{N}}$ (here $\Re$ and $\Im$ indicate real and imaginary parts; see main text for the definitions of these coupling terms). Using this parametrization, one can readily compute the Chern number $\mathscr{C}_{\mathrm{L}}$, a topological invariant that, due to the bulk-edge correspondence[49], yields the (integer) number of edge states per quasimomentum under open boundary conditions (OBC) lying in the gap of the spectrum of $\mathscr{H}_{\mathrm{L}}$, or alternatively $H(\mathbf{k})$, whose energy bands are given by

$$\epsilon(\mathbf{k}) = f(\mathbf{k}) \pm |\mathbf{d}(\mathbf{k})| \tag{5}$$

Defining the unit vector $\hat{\mathbf{d}}(\mathbf{k}) = \mathbf{d}(\mathbf{k})/|\mathbf{d}(\mathbf{k})|$, $\mathscr{C}_{\mathrm{L}}$ can be calculated as an integral in $\mathbf{k}$-space[40]

$$\mathscr{C}_{\mathrm{L}} = \int_{-\pi}^{\pi} \mathrm{d}k_x \int_{-\pi}^{\pi} \mathrm{d}k_y \mathscr{B}(k_x, k_y) \tag{6}$$

where the Berry curvature in terms of $\hat{\mathbf{d}}(\mathbf{k})$ is given by $\mathscr{B} = 1/4\pi\hat{\mathbf{d}}\cdot(\partial_{k_x}\hat{\mathbf{d}} \times \partial_{k_y}\hat{\mathbf{d}})$. The simplicity of the parametrization in equations (4a)–(4d) affords an analytical expression for $\mathscr{C}_{\mathrm{L}}$ in equation (6), given by

$$\mathscr{C}_{\mathrm{L}} = \frac{\text{Numerator}}{\text{Denominator}}$$

$$\begin{aligned}\text{Numerator} = {} & (A_2B_1 - A_1B_2)[C_1\cos(2k_x) \\ & + (C_1 - C_2)(-3 + 2\cos(k_x)\cos(k_y)) - C_2\cos(2k_y)]\end{aligned}$$

$$\begin{aligned}\text{Denominator} = 32\pi\Big\{ & [C_1\cos(k_x) + C_2\cos(k_y)]^2 + \frac{1}{2}[(A_2^2 + B_2^2)(1 + \cos(k_x - k_y)) \\ & + 2(A_1A_2 + B_1B_2)(\cos(k_x) + \cos(k_y)) \\ & + (A_1^2 + B_1^2)(1 + \cos(k_x + k_y))]\Big\}^{3/2}\end{aligned} \tag{7}$$

The sign of $\mathscr{C}_{\mathrm{L}}$ indicates the chirality of the edge state and topologically non-trivial phases are characterized by a nonvanishing C_{L}.

A word of caution follows about the correct interpretation of $\mathscr{C}_{\mathrm{L}}$ in the context of this exciton problem, besides the one already given. First, were $\mathscr{H}_{\mathrm{L}}$ to describe an electronic rather than an exciton problem, not every band structure given by equation (5) satisfies the condition of an electronic insulator: owing to the $\mathbf{k}$-dependent offset $f(\mathbf{k})$, there is not always an gap where one can place the Fermi energy such that it does not cross any of the bulk bands. This issue deteriorates topological protection, allowing scattering into the bulk. However, for the cases that qualify as an insulator, such as the example described in the main text, $\mathscr{H}_{\mathrm{L}}$ represents a Chern insulator which exhibits a quantized transverse conductance $e^2/h\mathscr{C}_{\mathrm{L}}$ (e is charge of an electron and h is Planck's constant) under a weak voltage bias, giving an experimental interpretation to the meaning of $\mathscr{C}_{\mathrm{L}}$ (ref. 40). Our case is different, as we are limiting ourselves to single-excitation effects, rather than considering a macroscopic occupation of the states, as in an actual electronic insulator, and the occupation of the bands occurs through light and not through a difference in electrochemical potential. Yet, it is an intriguing problem to find an excitonic observable that directly corresponds to $\mathscr{C}_{\mathrm{L}}$. One could imagine designing a protocol that occupies the edge states and not the bulk bands, and which applies a bias potential to the excitons via, say, mechanical strain[50]. The measurement of an exciton current in this situation would be related to $\mathscr{C}_{\mathrm{L}}$. As noted in the main text, a more careful description of such an experimental protocol involving near-field spectroscopic techniques will be defined in the extension of this work; for now, we will content ourselves with the first interpretation of $\mathscr{C}_{\mathrm{L}}$ in terms of the number of edge states. Even though everything in this section referred to $\mathscr{H}_{\mathrm{L}}$, the analogous conclusions apply to $\mathscr{H}_{\mathrm{U}}$. In fact, one can easily show that equation (7) is also valid for $\mathscr{C}_{\mathrm{U}}$, provided the corresponding dipolar couplings are used.

Finally, we shall discuss some symmetries of $\mathscr{C}_{\mathrm{v}}$. In the text, we argued that $\mathscr{C}_{\mathrm{L}} = -\mathscr{C}_{\mathrm{U}}$. This claim can be restated as $\mathscr{C}_{\mathrm{v}}$ changing sign on switching the + and − labels, $\{|Q_+^{(i)}\rangle, |Q_-^{(i)}\rangle\} \leftrightarrow \{|Q_-^{(i)}\rangle, |Q_+^{(i)}\rangle\}$. By keeping track of the various matrix elements, we can see that $\mathscr{C}_{\mathrm{v}}$ also reverses sign on the transformation $\kappa_i \leftrightarrow -\kappa_i$ across both sublattices. However, inverting the projection of the magnetic field on the porphyrins, $\kappa_i \leftrightarrow -\kappa_i$, also reassigns the upper and lower energy states $|Q_{\mathrm{L}}^{(i)}\rangle$ and $|Q_{\mathrm{U}}^{(i)}\rangle$ between $|Q_+^{(i)}\rangle$ and $|Q_-^{(i)}\rangle$, switching + and − labels. Hence, the value of $\mathscr{C}_{\mathrm{L}}$ (and consequently, of $\mathscr{C}_{\mathrm{U}}$) is fixed across tilting configurations, and by computation seen to correspond to $\mathscr{C}_{\mathrm{L}} = -1$ for $B_z > 0$. Because B_z also switches + and −, $\mathscr{C}_{\mathrm{L}} = 1$ for $B_z < 0$.

Received 9 March 2014; accepted 31 July 2014; published online 21 September 2014

References

1. Davydov, A. *Theory of Molecular Excitons* (McGraw-Hill, 1962).
2. Gregg, B. A. Excitonic solar cells. *J. Phys. Chem. B* **107,** 4688–4698 (2003).
3. Scholes, G. D. & Rumbles, G. Excitons in nanoscale systems. *Nature Mater.* **5,** 683–696 (2006).
4. Saikin, S. K., Eisfeld, A., Valleau, S. & Aspuru-Guzik, A. Photonics meets excitonics: Natural and artificial molecular aggregates. *Nanophotonics* **2,** 21–38 (2013).
5. Kippelen, B. & Bredas, J-L. Organic photovoltaics. *Energy Environ. Sci.* **2,** 251–261 (2009).
6. Fidder, H., Knoester, J. & Wiersma, D. A. Optical properties of disordered molecular aggregates: A numerical study. *J. Chem. Phys.* **95,** 7880–7890 (1991).
7. Mohseni, M., Rebentrost, P., Lloyd, S. & Aspuru-Guzik, A. Environment-assisted quantum walks in photosynthetic energy transfer. *J. Chem. Phys.* **129,** 174106 (2008).
8. Plenio, M. B. & Huelga, S. F. Dephasing-assisted transport: Quantum networks and biomolecules. *New J. Phys.* **10,** 113019 (2008).
9. Cao, J. & Silbey, R. J. Optimization of exciton trapping in energy transfer processes. *J. Phys. Chem. A* **113,** 13825–13838 (2009).
10. Yoshioka, D. *The Quantum Hall Effect* (Springer, 1998).
11. Halperin, B. I. Quantized Hall conductance, current-carrying edge states, and the existence of extended states in a two-dimensional disordered potential. *Phys. Rev. B* **25,** 2185–2190 (1982).
12. Wang, Z., Chong, Y., Joannopoulos, J. D. & Soljacic, M. Observation of unidirectional backscattering-immune topological electromagnetic states. *Nature* **461,** 772–775 (2009).
13. Rechtsman, M. C. *et al.* Photonic floquet topological insulators. *Nature* **496,** 196–200 (2013).
14. Hafezi, M., Mittal, S., Fan, J., Migdall, A. & Taylor, J. M. Imaging topological edge states in silicon photonics. *Nature Photon.* **7,** 1001–1005 (2013).
15. Khanikaev, A. B. *et al.* Photonic topological insulators. *Nature Mater.* **12,** 233–239 (2013).
16. Hasan, M. Z. & Kane, C. L. Colloquium: Topological insulators. *Rev. Mod. Phys.* **82,** 3045–3067 (2010).
17. Qi, X. & Zhang, S-C. Topological insulators and superconductors. *Rev. Mod. Phys.* **83,** 1057–1110 (2011).
18. Wang, Z. F., Su, N. & Liu, F. Prediction of a two-dimensional organic topological insulator. *Nano Lett.* **13,** 2842–2845 (2013).
19. Wang, Z. F., Liu, Z. & Liu, F. Organic topological insulators in organometallic lattices. *Nature Commun.* **4,** 1471 (2013).
20. Liu, Z., Wang, Z. F., Mei, J. W., Wu, Y. S. & Liu, F. Flat Chern band in a two-dimensional organometallic framework. *Phys. Rev. Lett.* **110,** 106804 (2013).
21. Wang, Z. F., Liu, Z. & Liu, F. Quantum anomalous Hall effect in 2D organic topological insulators. *Phys. Rev. Lett.* **110,** 196801 (2013).
22. Kim, D. (ed.) *Multiporphyrin Arrays: Fundamentals and Applications* (Pan Stanford, 2012).
23. Martinez-Diaz, M. V., de la Torre, G. & Torres, T. Lighting porphyrins and phthalocyanines for molecular photovoltaics. *Chem. Commun.* **46,** 7090–7108 (2010).

24. Suto, K., Yoshimoto, S. & Itaya, K. Two-dimensional self-organization of phthalocyanine and porphyrin: Dependence on the crystallographic orientation of Au. *J. Am. Chem. Soc.* **125,** 14976–14977 (2003).
25. Barrena, E., de Oteyza, D. G., Dosch, H. & Wakayama, Y. 2D supramolecular self-assembly of binary organic monolayers. *ChemPhysChem* **8,** 1915–1918 (2007).
26. Brede, J. *et al.* Dynamics of molecular self-ordering in tetraphenyl porphyrin monolayers on metallic substrates. *Nanotechnology* **20,** 275602 (2009).
27. Gao, A. *et al.* Two-dimensional self-assembly of a porphyrin–polypyridyl ruthenium(II) hybrid on HOPG surface through metal–ligand interactions. *ChemPhysChem* **11,** 1951–1955 (2010).
28. Birnbaum, T. *et al.* Optical and magneto-optical properties of metal phthalocyanine and metal porphyrin thin films. *J. Phys. Condens. Matter.* **26,** 104201 (2014).
29. Feyer, V. *et al.* Adsorption geometry and electronic structure of iron phthalocyanine on Ag surfaces: A LEED and photoelectron momentum mapping study. *Surf. Sci.* **621,** 64–68 (2014).
30. Maier, S. *et al.* Nanoscale engineering of molecular porphyrin wires on insulating surfaces. *Small* **4,** 1115–1118 (2008).
31. Scarfato, A. *et al.* Scanning tunneling microscope study of iron(II) phthalocyanine growth on metals and insulating surfaces. *Surf. Sci.* **602,** 677–683 (2008).
32. Malley, M., Feher, G. & Mauzerall, D. The Zeeman effect in porphyrins. *J. Mol. Spectrosc.* **26,** 320–334 (1968).
33. Villamaina, D., Bhosale, S. V., Langford, S. J. & Vauthey, E. Excited-state dynamics of porphyrin–naphthalenediimide–porphyrin triads. *Phys. Chem. Chem. Phys.* **15,** 1177–1187 (2013).
34. Canters, C. G. & van der Waals, J. H. in *The Porphyrins* Vol. 3 (ed. Dolphin, D.) Ch. 12, 531–582 (Academic, 1978).
35. Rodriguez, J. J. & Mukamel, S. Zeeman shift of two-dimensional optical signals of Mg-porphyrin dimers with circularly polarized beams. *J. Chem. Phys.* **137,** 205102 (2012).
36. Kadish, K. M., Smith, K. M. & Guilard, R. (eds) *Handbook of Porphyrin Science* (World Scientific, 2010).
37. Yao, N. Y. *et al.* Topological flat bands from dipolar spin systems. *Phys. Rev. Lett.* **109,** 266804 (2012).
38. Yao, N. Y. *et al.* Realizing fractional Chern insulators in dipolar spin systems. *Phys. Rev. Lett.* **110,** 185302 (2013).
39. Haldane, F. D. M. Model for a quantum Hall effect without Landau levels: Condensed-matter realization of the 'parity anomaly'. *Phys. Rev. Lett.* **61,** 2015–2018 (1988).
40. Thouless, D. J., Kohmoto, M., Nightingale, M. P. & den Nijs, M. Quantized Hall conductance in a two-dimensional periodic potential. *Phys. Rev. Lett.* **49,** 405–408 (1982).
41. Knoester, J. Modeling the optical properties of excitons in linear and tubular J-aggregates. *Int. J. Photoenergy* **2006,** 61364 (2006).
42. Sánchez, E. J., Novotny, L. & Xie, X. S. Near-field fluorescence microscopy based on two-photon excitation with metal tips. *Phys. Rev. Lett.* **82,** 4014–4017 (1999).
43. Akselrod, G. M. *et al.* Visualization of exciton transport in ordered and disordered molecular solids. *Nature Commun.* **5,** 3646 (2014).
44. Sheberla, D. *et al.* High electrical conductivity in Ni_3(2,3,6,7,10,11-hexaiminotriphenylene)$_2$, a semiconducting metal-organic graphene analogue. *J. Am. Chem. Soc.* **136,** 8859–8862 (2014).
45. Zimborás, Z. *et al.* Quantum transport enhancement by time-reversal symmetry breaking. *Sci. Rep.* **3,** 2361 (2013).
46. Lu, D. *et al.* Chiral quantum walks. Preprint http://arxiv-org/abs/1405.6209 (2014).
47. Fu, L. Topological crystalline insulators. *Phys. Rev. Lett.* **106,** 106802 (2011).
48. Hsieh, T. H. *et al.* Topological crystalline insulators in the SnTe material class. *Nature Commun.* **3,** 982 (2012).
49. Bernevig, B. A. *Topological Insulators and Topological Superconductors* (Princeton Univ. Press, 2013).
50. Feng, J., Qian, X., Huang, C-W. & Li, J. Strain-engineered artificial atom as a broad-spectrum solar energy funnel. *Nature Photon.* **6,** 866–872 (2012).

Acknowledgements

J.Y-Z. is grateful to B. Halperin, I. Kassal, and X. Andrade for discussions, and to O. Starykh for kindly sharing his notes on the subject. All the authors would like to thank C. Laumann for discussions at the early stages of the project. J.Y-Z. and A.A-G. are supported by an Energy Frontier Research Center funded by the US Department of Energy, Office of Science, Office of Basic Energy Sciences under Award Number DESC0001088. N.Y. acknowledges support from the Department of Energy (FG02-97ER25308). Finally, S.K.S. and A.A-G. are supported by the Defense Threat Reduction Agency grant HDTRA1-10-1-0046.

Author contributions

All authors contributed to the results presented in this Article.

Additional information

Reprints and permissions information is available online at www.nature.com/reprints. Correspondence and requests for materials should be addressed to J.Y-Z.

Competing financial interests

The authors declare no competing financial interests.